

Positive and Negative Charge Carriers in Doped or Photoexcited Polydithienothiophenes: A Comparative Study Using Raman, Infrared, and Electron Spin Resonance Spectroscopy

Antonio Cravino,^{*,†} Helmut Neugebauer,[†] Silvia Luzzati,[‡] Marinella Catellani,[‡] Andreas Petr,[§] Lothar Dunsch,[§] and N. Serdar Sariciftci[†]

Linz Institute for Organic Solar Cells (LIOS), Physical Chemistry, Johannes Kepler University Linz, Altenbergerstrasse 69, A-4040 Linz, Austria, Istituto di Chimica delle Macromolecole, Consiglio Nazionale delle Ricerche, Via Bassini 15, I-20133 Milano, Italy, and Institut für Festkörper- und Werkstofforschung, Institut für Festkörperforschung, Abteilung Elektrochemie und Leitfähige Polymere, Helmholtzstrasse 20, D-01069 Dresden, Germany

Received: August 29, 2001; In Final Form: January 17, 2002

Poly(dithienothiophene)s (PDTTs), low band-gap conjugated polymers with polythiophene-like chain where an aromatic thienothiophene moiety is fused to each thiophene ring, were studied using Raman spectroscopy, photoinduced infrared absorption, as well as attenuated total reflection Fourier transform infrared (ATR-FTIR) and electron spin resonance (ESR) spectroelectrochemistry. The spectroelectrochemical studies were performed in situ during p- and n-doping (electrochemical oxidation and reduction, respectively). Raman lines of the pristine polymers are compared to infrared active vibration (IRAV) bands due to the charge carriers injected by the electrochemical doping processes or by illumination. The different π -electron distribution along the polythiophene-like chain, which determines the different band-gap sizes, also account for the different lattice relaxations and vibrational behaviors shown by these polymers. By means of in situ ESR spectroscopy, the formation of paramagnetic positive and negative charge carriers with unusually high g-factors could be proved.

Introduction

Due to a strong lattice relaxation in one-dimensional systems with strong electron–phonon coupling,^{1,2} chemical as well as electrochemical oxidation and reduction of nondegenerate ground-state conjugated polymers usually lead to the formation of charge carriers with spin 1/2, denoted as positive/negative polarons (radical-cations/-anions), delocalized along the polymer chain and which exhibit peculiar electronic, vibrational, and charge transport properties.^{1,3} Also, photoexcitations may lead to charge separation and to the formation of such charge carriers.^{1,4,5} The lattice relaxation induces new electronic levels within the polymer π – π^* energy gap (band-gap) and usually lead to an insulator-to-metal transition at a critical doping level. The redox processes involving the formation of charge carriers in conjugated polymers are described, in analogy to inorganic semiconductors, as p-, n-, and photodoping.

Due to the strong electron–phonon coupling in conjugated polymers, Raman spectroscopy and infrared absorption are powerful techniques for the investigation of the doping induced lattice relaxation around the charge carriers. Consequently, the vibrational behavior of relatively simple conjugated polymers in their pristine and doped states (mostly of the p-type) has been the subject of much theoretical and experimental work during the last two decades.^{6–14} On the other hand, detailed studies of

more complicated or *n-doped* conjugated polymers have been limited by theoretical difficulties and by their frequent instability, respectively.

The infrared spectra of conjugated polymers in their conductive (chemically- or photodoped) states are characterized by intense IRAV bands, typically ranging from 1600 to 700 cm^{-1} .⁶ These bands originate from the strong electron–phonon coupling mentioned above and thus provide not only structural but also electronic information. In addition, IRAVs are usually accompanied by broad IR absorption bands at higher energy. These bands correspond to the transitions involving the in-the-gap electronic levels.

Several theoretical models have been developed in order to explain the spectroscopic signatures of charge carriers. For the description of the electronic and vibrational properties of neutral and doped *trans*-polyacetylene, Horovitz et al. and Ehrenfreund et al. have considered the change in the charge density wave associated to the vibrational motion of the polymer backbone.^{8,9} As quantification of the localization of charge a “pinning parameter” was introduced. Zerbi et al. explained the IRAV bands by the IR activation of the Raman active A_g modes in the pristine form of the polymer due to the local breaking of the symmetry around the charge carrier.^{6,10,11} In this model, the high intensity of the IRAV bands is motivated by the large variation of the electric dipole momentum associated to the oscillation of the charged defect. An “effective conjugation coordinate” (ECC) describes the changes in geometry going from the ground- to the excited-state of the polymer as an alternate stretching–shrinking of carbon–carbon bonds. The higher the contribution of a given mode to the ECC, the higher is the intensity of the corresponding IRAV band. This origin of the IRAV bands shows that both Raman spectroscopy and IR

* To whom correspondence should be addressed. Tel: +43-732-2468-8767. Fax: +43-732-2468-8770. E-mail: antonio.cravino@jku.at.

[†] Linz Institute for Organic Solar Cells (LIOS), Physical Chemistry, Johannes Kepler University Linz.

[‡] Istituto di Chimica delle Macromolecole, Consiglio Nazionale delle Ricerche.

[§] Institut für Festkörper- und Werkstofforschung, Institut für Festkörperforschung, Abteilung Elektrochemie und Leitfähige Polymere.

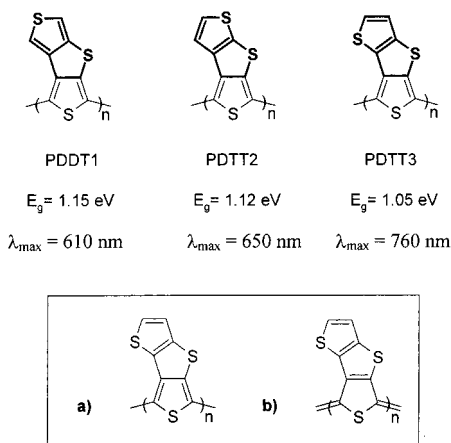


Figure 1. Chemical structures, band-gap values (E_g) and maximum absorption wavelengths (λ_{max}) of PDTTs. E_g and λ_{max} data from ref 16. The inset show the relevant canonical forms: (a) aromatic; (b) quinoidal.

spectroscopy as complementary techniques are necessary for understanding the vibrational spectra of pristine and doped conjugated polymers. Recently, Ehrenfreund and Vardeny used a model introduced by Giraldo et al. (GPS model)¹² to establish a link between the electronic absorption bands and the IRAV bands of doping induced spectra.¹³ All of the models correlate intensity, width, and position of the IRAV bands to the delocalization of charge carriers along the polymer chain.

These theories, developed for relatively simple systems such as *trans*-polyacetylene and extended to few polyheteroaromatics, do not account for possible differences in the IRAV signatures of positive and negative charge carriers. In addition, because the “pinning” in absence of counterions should be lower, photoinduced IRAV bands should appear at lower wavenumbers than chemically induced bands.¹⁵ Experimental work has confirmed that these models rationalize the spectroscopic behavior of conjugated polymers, providing a self-consistent description of the vibrational properties of many and relatively simple systems like, for instance, poly(alkylthiophene)s.^{6,14} However, some conjugated polymers show a more complex behavior. These materials are often promising candidates for applications because they may combine low band gap, outstanding optical properties and high stability in either the p- and n-doped states. A detailed description of the electronic and vibrational properties of such materials is necessary for the basic understanding of their behavior. In particular, spectroscopic studies of conjugated polymers with stable n-doped state might be useful to achieve better experimental and theoretical descriptions of the so far rarely observed negative charge carriers in conjugated polymers.

The low band gap and both the p- and n-dopability of the polydithienothiophenes (PDTTs) poly(dithieno[3,4-b:3',4'-d]thiophene) (PDTT1), poly-(dithieno[3,4-b:3',2'-d]thiophene) (PDTT2), and poly-(dithieno[3,4-b:2',3'-d]thiophene) (PDTT3)^{16–19} make them attractive for comparative spectroscopic studies of doping induced defects. The polymer structures are shown in Figure 1 along with their band-gap values.¹⁶ According to Bolognesi and co-workers²⁰ and ref 21, PDTT1, PDTT2, and PDTT3 can be regarded as polythiophene-like chains in which a thienothiophene aromatic moiety,^{22,23} evidenced by bold bonds in Figure 1, is fused to each thiophene ring. PDTTs have been prepared following the idea that an aromatic system fused to the thiophene ring lying in the polythiophene-like chain increases the quinoidal character of the latter and, therefore, the π -electron inter-ring delocalization along the whole polymer (see inset in Figure 1, where PDTT3

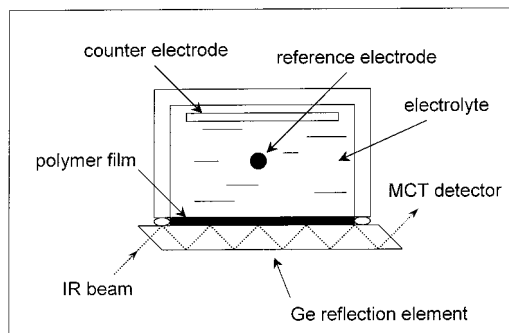


Figure 2. Spectroelectrochemical cell for in situ ATR-FTIR spectroscopy.

is sketched as example).^{24–26} Indeed, according to this synthetic principle, PDTT1, PDTT2, and PDTT3 show low band-gap values. The higher the aromaticity of the fused thienothiophene moiety, which increases in the sequence PDTT1, PDTT2, PDTT3,²³ the lower is the polymer band-gap size. Due to the electron–phonon coupling in conjugated polymers, different moieties fused to the same polythiophene-like chain are expected to influence also the vibrational behavior of PDTT1, PDTT2, and PDTT3. By means of Raman spectroscopy, in situ attenuated total reflection (ATR) FTIR spectroelectrochemistry and photoinduced FTIR absorption spectroscopy, we have indeed observed that these members of the same polymer family exhibit a variety of spectroscopic behaviors. In particular, PDTT1 and PDTT2 in their p- and n-doped states show two dissimilar IRAV patterns. Conversely, no substantial differences are found between the spectra of p- and n-doped PDTT3. In all cases, the photoinduced IR absorption spectra resemble those of the p-doped polymer and do not show softening of modes, indicating that a kind of pinning occurs even in absence of electrolyte counterions.

Electron spin resonance (ESR) combined with electrochemistry has been applied successfully in the elucidation of the doping mechanisms of several conjugated polymers and can directly proof the formation of paramagnetic charge carriers such as polarons.^{27–30} In situ ESR spectroelectrochemistry measurements performed during p- and n-doping of PDTT1, PDTT2 and PDTT3 reveal that the charge carriers of polaronic nature exhibit unusually high *g*-factors. In addition, negative polarons have systematically higher *g*-factors as compared to their positive counterparts.

Experimental Section

The monomers DTT1, DTT2, and DTT3 were synthesized following methods reported in the literature.^{31,32} For electropolymerization, the monomers were dissolved, working in an argon drybox and using shielded glassware, in anhydrous acetonitrile containing tetrabutylammonium hexafluorophosphate (0.1 M) as supporting electrolyte. The solution was then transferred via syringe into the spectroelectrochemical cell sketched in Figure 2. A platinumized Ge reflection element with an electrochemically active area of 0.63 cm² was the working electrode, whereas a Pt foil and a Ag/AgCl wire electrode (−190 mV vs SCE) were the counter and the quasi-reference electrode, respectively. The electrochemical equipment consisted of a Jaisle 1002T-NC potentiostat, a Prodis 1/14 I sweep generator and a Rikadenki RY-PIA x-y recorder. Thin films of the polymers were electrosynthesized potentiostatically according to Arbizzani et al.¹⁶ After electrosynthesis, the spectroelectrochemical cell was rinsed with a monomer-free electrolyte solution. Prior of in-situ ATR-FTIR spectroelectrochemistry, the polymer films

were electrochemically dedoped. The same procedure was performed, followed by washing and drying steps, prior of the photoinduced PIA-FTIR absorption and ESR measurements done as described below. To prevent side reactions due to oxygen and/or moisture, the experiments were done under argon. During potential cycling at a sweep rate of 5 mV/s, infrared spectra were recorded consecutively. Each spectrum results from 32 scans and covers a range of about 90 mV in the corresponding cyclic voltammogram. Spectral changes during doping were obtained by selecting a spectrum, recorded just before the investigated process, as reference and then relating the subsequent spectra to this chosen reference. Spectra were calculated as $\Delta[-\log T_{\text{ATR}}]$, where T_{ATR} is the transmittance in the ATR geometry. Details and the setup for in-situ ATR-FTIR spectroelectrochemistry have been described elsewhere.^{33–35}

For PIA-IR spectroscopy the samples were mounted on the coldfinger of a liquid nitrogen cooled cryostat with ZnSe windows and illuminated in a 45° geometry. The excitation was made by the 488 nm line of an Ar⁺ laser, with intensity of 30 mW/cm². The PIA infrared spectrum was obtained by recording 10 single beam spectra under illumination followed by 10 single beam spectra recorded in the dark. 300 repetitions of this sequence were accumulated to achieve a satisfying signal-to-noise ratio.

For Raman measurements the polymer films have been electrodeposited on indium-thin oxide coated glass (Balzer, resistivity 20 ohms/□) electrodes and then again carefully dedoped. The spectra were recorded with a Bruker IFS 66+FRA 106 FT spectrometer working with a Nd:YAG laser, when excitation was made in the near-IR (NIR) and with a flat field monochromator Jasco TRS 300 equipped with an EG&G intensified diode array OMA 1420, using Ar⁺ and He-Ne laser lines at 457, 488, 514, and 633 nm, when excitation was made in the visible. Raman measurements were carried out at room temperature and under argon. IR and Raman spectra were recorded with resolution of 4 cm⁻¹.

For in situ ESR experiments, a X-band spectrometer ESP300E (Bruker) was used. All measurements were carried out at room temperature with 100 kHz modulation and at microwave power of 2 mW. The standard cavity ER 4104 OR (Bruker) resonant in the TE₁₀₂ mode was used. The spectroelectrochemical ESR flat cell has been described in detail elsewhere.³⁶ During potential cycling at a rate of 10 mV/s, ESR spectra were recorded consecutively. As standard, a capillary filled with magnesium oxide containing Mn²⁺ was fixed outside of the spectroelectrochemical cell.

Results and Discussion

Raman Spectroscopy. Resonant Raman scattering is an useful tool to obtain some insight on how the different thienothiophene moieties are affecting the π -electron delocalization of the polythiophene-like conjugated backbone. The resonant Raman spectra obtained at various excitation wavelengths are displayed in Figure 3, 4 and 5. In the following discussion, α , β , and γ refer to PDTT1, PDTT2, and PDTT3, respectively. Upon tuning the excitation wavelength within the polymer $\pi \rightarrow \pi^*$ absorption bands (for absorption spectra see ref 16), the selective excitation of chain segments with different π -electron delocalization leads to a frequency dispersion and to an intensity redistribution of the Raman modes. At lower excitation wavelengths, i.e., in resonance with the shortest conjugation lengths, PDTTs exhibit two intense Raman bands, indexed 1 and 2 (Figure 3(a–d), Figure 4(a–c) and Figure 5

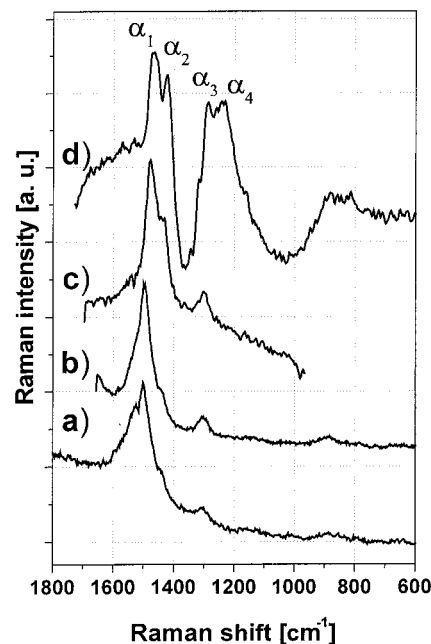


Figure 3. Raman spectra of pristine PDTT1. Excitation at 457 (a), 488 (b), 633 (c), and 1064 nm (d).

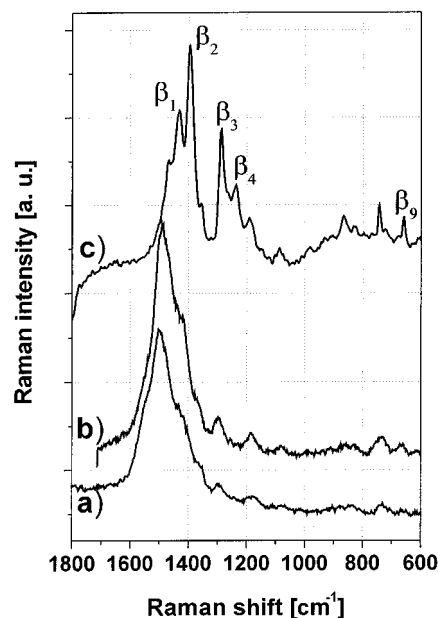


Figure 4. Raman spectra of pristine PDTT2. Excitation at 457 (a), 514 (b), and 1064 nm (c).

(a–d). See also Table 1). With the NIR excitation ($\lambda = 1064$ nm) near the onset of the absorption band of PDTTs,¹⁶ and thus, in resonance with the chain segments with the more extended π -electron delocalization, the Raman spectra display a much more complicated pattern. The PDTT1 Raman spectrum (Figure 3(d)) shows four relevant bands at 1466 (α_1), 1422 (α_2), 1287 (α_3), 1237 cm⁻¹ (α_4); a broad and weaker feature is seen at about 850 cm⁻¹. The Raman spectrum of PDTT2 (Figure 4(c)) is rather similar to that of PDTT1. Although red-shifted, the intense bands seen at 1431 (β_1) and 1395 (β_2) cm⁻¹ compare well with α_1 and α_2 . Again, two bands are at 1287 (β_3) and 1237 cm⁻¹ (β_4). The most striking difference is the presence of several medium or weak bands below 1000 cm⁻¹ (β_5 – β_9 , listed in Table 2). For PDTT3, detailed data have been reported recently.³⁷ Its NIR excitation spectrum (Figure 5(d)) shows a quite complicated pattern, in which five main bands are observed

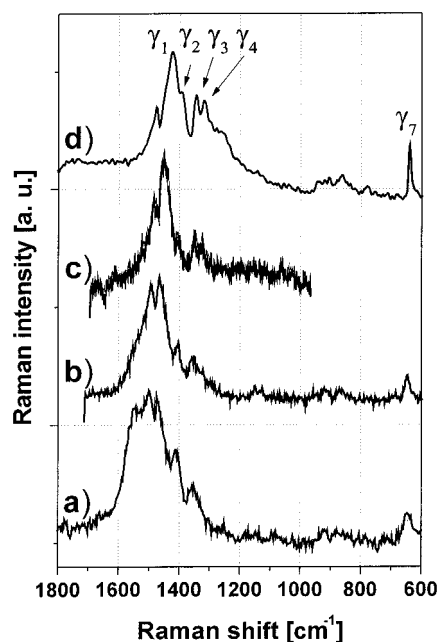


Figure 5. Raman spectra of pristine PDTT3. Excitation at 457 (a), 514 (b), 633 (c), and 1064 nm (d).

TABLE 1: Band Assignment and Wavenumber of Raman and IRAV Modes

	PDTT1				
	$\bar{\nu}(\alpha_1)$	$\bar{\nu}(\alpha_2)$	$\bar{\nu}(\alpha_3)$	$\bar{\nu}(\alpha_4)$	$\bar{\nu}(\alpha_5)$
457 nm	1501	sh	1303		vw
488 nm	1495	1440 sh	1300		vw
633 nm	1479	1437 sh	1298		/
1064 nm	1466	1422	1287	1237	~850 w
p	1438 w	1361	1277	1205	
n	1456 w	1385	1271	1207	
PIA	sh	1361	1278	1206	

	PDTT2								
	$\bar{\nu}(\beta_1)$	$\bar{\nu}(\beta_2)$	$\bar{\nu}(\beta_3)$	$\bar{\nu}(\beta_4)$	$\bar{\nu}(\beta_5)$	$\bar{\nu}(\beta_6)$	$\bar{\nu}(\beta_7)$	$\bar{\nu}(\beta_8)$	$\bar{\nu}(\beta_9)$
457 nm	1502	1437	vw		vw			vw	vw
514 nm	1490	1419	1295		1184	vw	vw	731	vw
1064 nm	1431	1395	1287	1237	1190	1086	866	743	658

	PDTT3							
	$\bar{\nu}(\gamma_0)$	$\bar{\nu}(\gamma_1)$	$\bar{\nu}(\gamma_2)$	$\bar{\nu}(\gamma_3)$	$\bar{\nu}(\gamma_4)$	$\bar{\nu}(\gamma_5)$	$\bar{\nu}(\gamma_6)$	$\bar{\nu}(\gamma_7)$
457 nm	1500	1473	1407	1355				646
514 nm	1495	1466	1402	1353	1331			646
633 nm	1485	1451	1402	1348	1325			/
1064 nm	1475	1422	1400 sh	1344	1318	1250 b	950–770	639
p (n)	1460	1401		1326	1287	1250-	950-	634
		1371			1120	1120	770	
PIA	1469	1400		1330	1295	1250-	950–770	634
		1372				1120		

Wavelengths are the Raman excitation lines; p, p-doping; n, n-doping; PIA, photodoping; w, weak; vw, very weak; sh, shoulder at 1475 (γ_0), 1422 (γ_1), 1344 (γ_3), 1318 (γ_4), and 639 (γ_7) cm^{-1} along with several weaker features. A remarkable behavior shows band γ_7 , which is assigned to modes containing C–S stretching character and located within the thienothiophene fused moiety.³⁷

These spectral features evidence that the Raman behavior of PDTTs is significantly different from that of simpler polythiophenes. In general, Raman spectra of the polythiophene family show three main lines coupled to the electronic transition. Two dominant lines are around 1500 and 1450 cm^{-1} (C=C stretching region),^{38,39} whereas a weaker feature is seen within

TABLE 2: IR Bands of Doped PDTTs^a

PDTT1 p	PDTT1 n	PDTT1 PIA
1687 vw		
1518 w	1525	
1438 vw	1456	
1361 vs	1385 vs	1361
1309 vw	1315 w	
1277 vs	1271 vs	1278
1205 vs	1207 m	1206
1157 w	1153 w	1151
1122	1111 w	
	929 w	1078
899 w		
845 vs el		
	760 vw	756
669 w		
644 w		630

PDTT2 p	PDTT2 n	PDTT2 PIA
1456 w	1450 w	
1392	1402	
1356 m	1349 ms	1363
1307		1317
1279		1276
	1249 vs	
1217 vs		1225
1178 m		
	1147 vs	
1082 s	1068 s	1082
922 mv		
837 vs el		
733 s sh	723 w	
690 mw		
659 w	651 m	657

PDTT3 p	PDTT3 n	PDTT3 PIA
1460 w	1469 w	1469
1445 vw		
1401 m	1403 m	1400
1371m	1369 m	1372
1326	1329 m	1330
1287 m	1281 s	1295
1214 s	1221 vs	1226
1180 s	1176 s	1180
1139 s	1150	1140
	1110 s	
1020	1080 m	
940 w		941
	891 m	862
842 vs el		
778 w	764 m	777
721 w	700 w	
684 w	660 w	
634 s	630 s	634

^a Numbers are wavenumbers, vs, very strong; s, strong; m, medium; w, weak; vw, very weak; el, electrolyte; p, p-doping; n, n-doping; PIA, photodoping

the range 1080–1050 cm^{-1} (C–C stretching + C–H wagging component).^{14,40} The modes that possess the largest ECC character correspond to the bands near 1500 cm^{-1} , which show a weak dispersion with different chain lengths (as well with different excitation wavelengths in polydispersed samples). This behavior is the vibrational signature proving that in polythiophenes π -electrons are mostly confined within each thiophene ring or within a very restricted domain of the chain.^{14,40} For PDTTs, significant differences to the simpler polythiophene Raman spectra are found:

–More complicated spectra are observed for PDTTs (more Raman lines are seen going from PDTT1 to PDTT2 and PDTT3);

—Most of the PDTTs Raman bands show both intensity redistribution and frequency dispersion with the excitation wavelength. The intense bands indexed 1 and 2 (see Figure 3(a–d), Figure 4(a–c), Figure 5(a–d) and Table 1) are identified as the modes with the largest ECC contribution which, as opposed to simple polythiophenes, exhibit a more relevant dispersion. Moreover, lines indexed 1 and 2 appear at significantly lower wavenumbers than the two lines near 1500 cm^{-1} in the simple polythiophenes' spectra;

—In PDTTs, no relevant Raman lines are observed around 1100 cm^{-1} ;

—In the region around 1300 cm^{-1} , no dominant lines are observed for polythiophenes, whereas two intense lines are seen for the PDTTs (band index 3 and 4).

Most of the above differences can be explained considering the enhanced weight of the quinoidal canonical form in the definition of the PDTTs electronic ground-state and hence the increased inter-ring electronic delocalization:

—This effect is overcoming the π -electron confinement found in polythiophenes (as well it is reducing the band-gap). Therefore, the modes containing the strongest ECC contribution do exhibit the predicted frequency dispersion;

—Apart from the relative differences in the weight of the canonical forms (crucial for the size of the band-gap), it is known that in both polythiophenes and PDTTs the ground-state is aromatic (the canonical structure a) in the inset of Figure 1 has the major weight in its definition).²¹ Therefore, the C=C stretching vibration mostly contributing to the ECC mode must be that between the nuclei $C_{\alpha}-C_{\beta}$ of the thiophene ring lying in the polythiophene-like chain. As such, the red-shift of lines 1 and 2 in PDTTs compared to the corresponding ECC modes in polythiophenes is motivated by the decrease of the $C_{\alpha}-C_{\beta}$ force constant that must accompany the increased quinoidal character of the chain. As further corroboration, these lines shift to lower wavenumbers as the polymer band-gap decreases ($\bar{\nu}(\alpha_1) > \bar{\nu}(\beta_1) > \bar{\nu}(\gamma_1)$ and $\bar{\nu}(\alpha_2) > \bar{\nu}(\beta_2), \bar{\nu}(\gamma_2)$);

—Conversely, the $C_{\alpha}-C_{\alpha'}$ (inter-ring bond) force constant should increase with increasing quinoidal character of the chain and, therefore, some bands should appear at higher wavenumber in the PDTT spectra than in those of polythiophenes. For the latter polymers, a medium band near 1200 cm^{-1} has been assigned to $C_{\alpha}-C_{\alpha'}$ symmetric stretching.^{38,39} Thus, it is noteworthy that PDTT spectra show intense lines, well above 1200 cm^{-1} , that shift to higher wavenumbers as the band-gap decreases ($\nu(\alpha_3) < \nu(\beta_3) < \nu(\gamma_3)$ and $\nu(\alpha_4) < \nu(\beta_4), \nu(\gamma_4)$).

In conclusion, the Raman spectra of PDTTs display the spectral signatures of an increased quinoidal character of the polythiophene-like chain compared to polythiophenes and of the involvement of the thienothiophene moieties to the polymer backbone π -electron delocalization. These effects are increasing from PDTT1 to PDTT2 to PDTT3.

In situ FTIR Spectroelectrochemistry. As mentioned in the Introduction, PDTT1, PDTT2, and PDTT3 are among the few conjugated polymers so far described that undergo both reversible p- and n-doping. A general and preferential way of doping is by electrochemistry, where the redox processes are determined by the electrode potential.^{41,42} In this way, a defined and reproducible doping can be obtained by the control of electrochemical parameters. By combining cyclic voltammetry and ATR-FTIR spectroscopy, we have recorded, in situ, the IR spectral changes during the doping processes of PDTT1, PDTT2, and PDTT3.

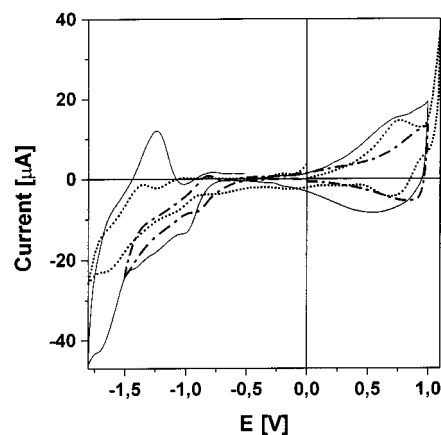


Figure 6. Cyclic voltammograms of PDTT1 (dash-dotted line), PDTT2 (dotted line), and PDTT3 (solid line), recorded during the in situ ATR-FTIR experiments. Scan rate 5 mV/s.

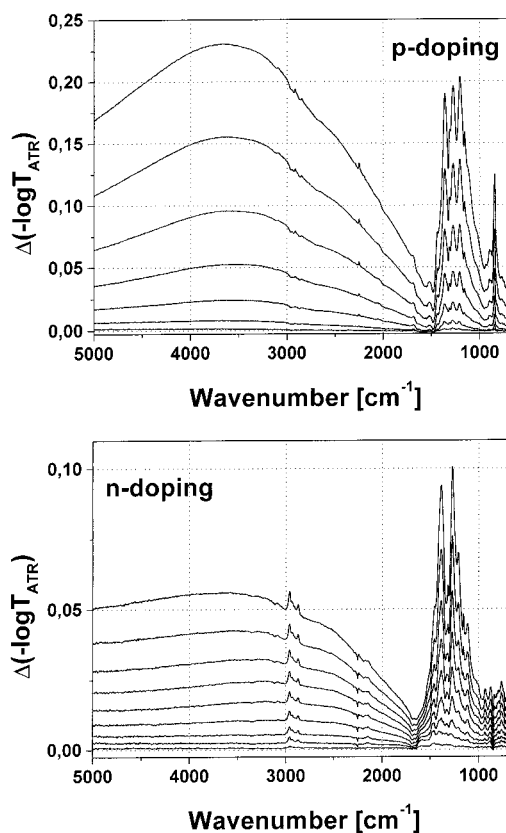


Figure 7. FTIR difference spectra during p- and n-doping of PDTT1. Sequence: bottom to top.

The cyclic voltammograms (scan rate 5 mV/s) taken during the in situ IR spectroelectrochemical experiments are shown in Figure 6.

The IR spectral changes developing during p- and n-doping of PDTT1 are depicted in Figure 7. With both p- and n-doping, the spectra show a broad electronic absorption band, with maximum around 3600 cm^{-1} , and IRAV bands in the vibrational range (the latter is represented in detail in Figure 8). The frequencies and the characteristics of the IRAV bands are reported, along with those observed upon doping of PDTT2 and PDTT3, in Table 2 (Table 2 collects also frequencies from the PIA-IR absorption spectra that will be discussed later). The sharp peak at 842 cm^{-1} , growing during the p-doping of all polymers, is due to the incorporation of the hexafluorophosphate ions balancing the charge formed on the polymer by the oxidation

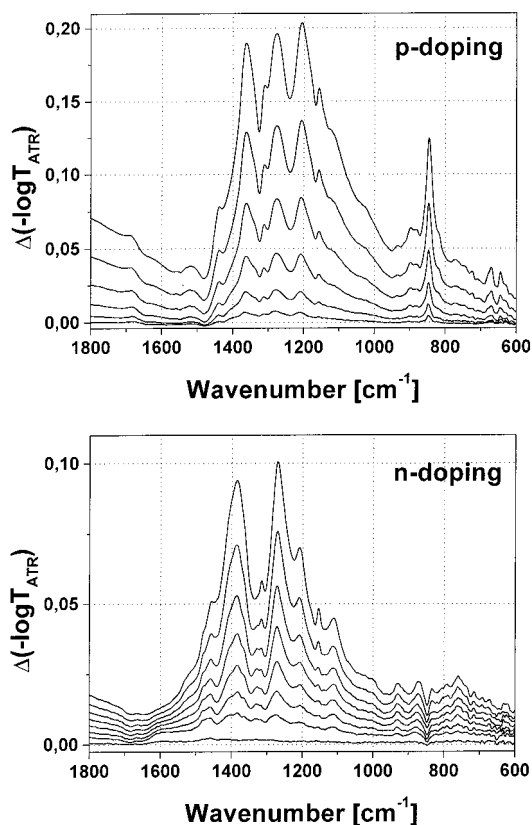


Figure 8. FTIR difference spectra during p- and n-doping of PDTT1. IRAV range. Sequence: bottom to top.

process. As can be seen, the following differences between p- and n-doped PDTT1 spectra are observed:

- The p-doped polymer spectrum shows three dominant IRAV bands, whereas only two intense IRAV bands emerge upon n-doping (Figure 8);

- In the n-doped polymer spectrum, the intensity of all features is about the 50% of that observed in the p-doped polymer spectrum (Figure 7);

- The relative intensities of bands are different in the two differently doped polymer forms. In particular, the intensity of the in-the-gap electronic absorption band relative to those of IRAV bands is drastically lower in the n-doped polymer spectrum (Figure 7).

A quite similar behavior shows PDTT2, whose spectra during p- and n-doping are depicted in Figure 9. Again, the spectral patterns include a broad electronic absorption band above 1500 cm^{-1} and IRAV bands in the vibrational range (detailed in Figure 10). Although the spectra are not as dissimilar as in the previous case, differences between the p- and n-doped polymer spectra are observed:

- p-doped PDTT2 shows an ill-defined IRAV spectrum due to the overlap of broad bands while the n-doped polymer spectrum clearly shows four intense IRAV bands (Figure 10);

- Remarkable differences are also seen when considering the features with medium and weak intensity below 800 cm^{-1} (Figure 10);

- Similar to PDTT1, the intensity of the n-doped PDTT2 bands is about 50% of those seen in the p-doped polymer spectrum.

Such differences indicate a different delocalization for the positive and negative charge carriers in PDTT1 and PDTT2, as already reported for other p- and n-dopable polymers such as poly(ethylene-2,3-dioxythiophene) (PEDOT)^{43–45} and poly-

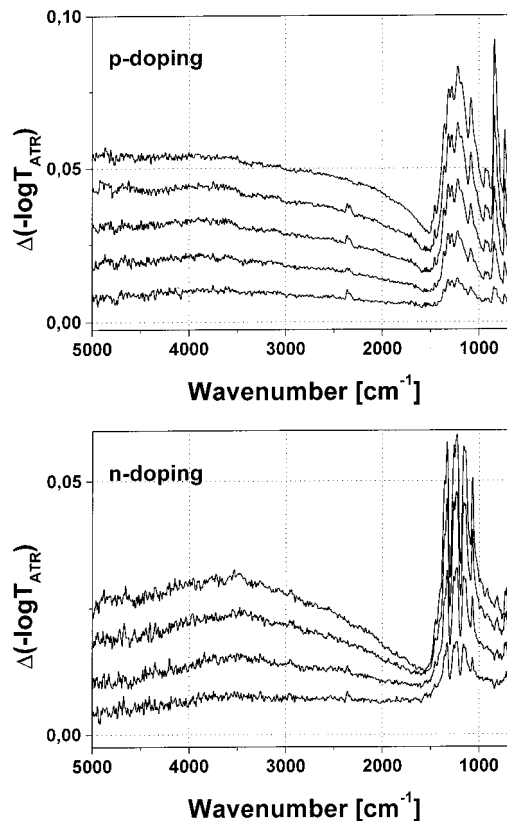


Figure 9. FTIR difference spectra during p- and n-doping of PDTT2. IRAV range. Sequence: bottom to top.

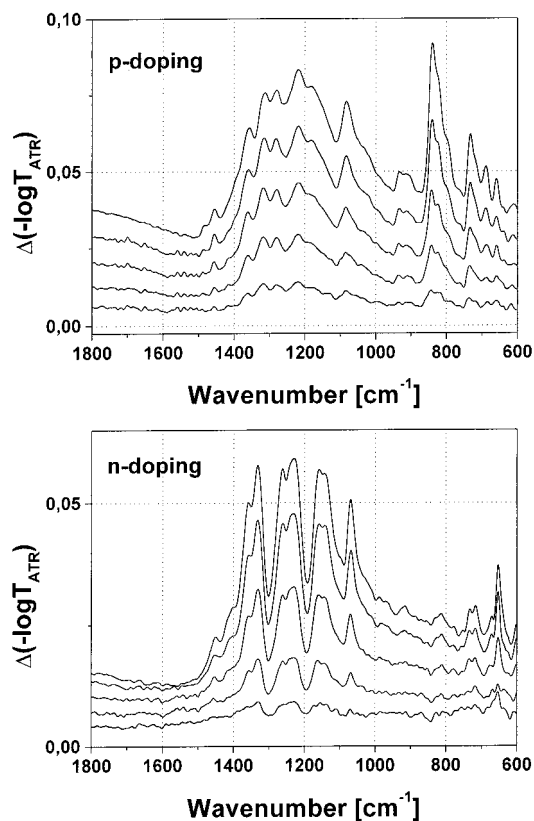


Figure 10. FTIR difference spectra during p- and n-doping of PDTT2. IRAV range. Sequence: bottom to top.

(isothianaphthemethine).⁴⁶ Despite the feasibility of reversible doping of both signs these polymers maintain a higher delocalization/mobility of positive charge carriers, as indicated by

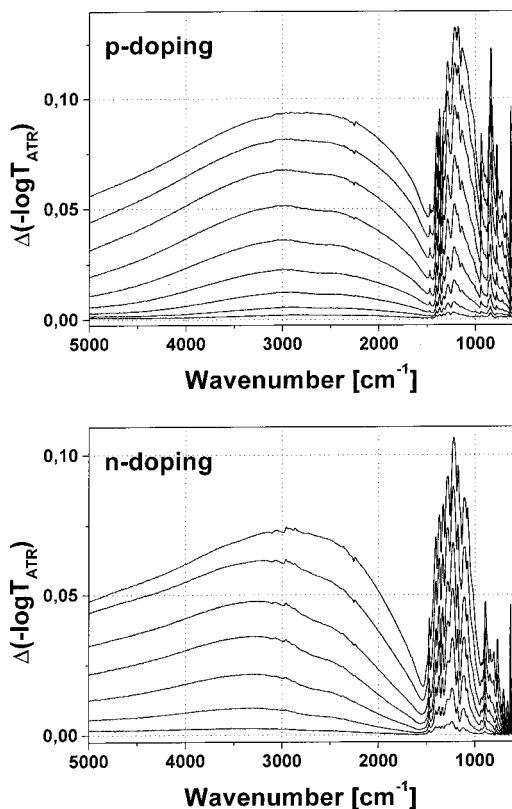


Figure 11. FTIR difference spectra during p- and n-doping of PDTT3. Sequence: bottom to top.

the higher intensity, the larger bandwidth and the lower wavenumber observed for the IRAV bands of the p-doped polymer forms as compared to the n-doped state.

For PDTT3, we have observed a different and peculiar behavior.^{37,45} Its p- and n-doped states show spectra (Figure 11 and Figure 12) in which almost no differences are observed, thus indicating rather similar structures and delocalization extension for charge carriers of both signs somehow suggesting potential bipolar transport properties, favorable for certain optoelectronic devices and photovoltaic applications.^{47–49}

Despite the polythiophene-like nature of the chain and as already observed by Raman spectroscopy, all of the p-doped PDTTs IR spectra do not compare well to those of simpler p-doped polythiophenes.^{6,50} Such a dissimilarity should not be observed if modes located within the fused thienothiophene moiety do not contribute significantly to the ECC. Within the PDTTs series, the results confirm that the π -electrons of the fused thienothiophene moiety of PDTTs affect differently the π -electron delocalization along the polythiophene-like chain, thus determining the different electronic and vibrational properties of the polymers. In particular, the fact that the spectral complexity increases from PDTT1 to PDTT2 and PDTT3, can be explained by the increased interaction between the π -electrons within the fused moiety and the polythiophene-like chain, according to the enhanced inter-ring delocalization as the band-gap decreases.

Photoinduced IR Absorption. The spectral signatures of charged carriers (electronic absorption and IRAV bands) are also observed in the photoinduced IR absorption spectra, which are presented in Figure 13 and in Figure 14 (band wavenumbers are collated in Table 2). The formation of both positive and negative charge carriers is expected by dissociation of exciton after photoexcitation as well as by direct excitation.⁵¹ However, it can be seen that the PIA-IR spectra are similar to those of

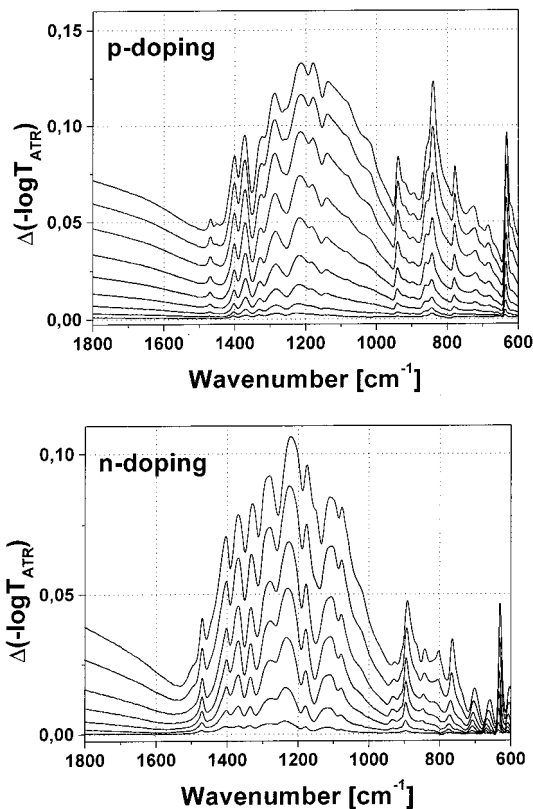


Figure 12. FTIR difference spectra during p- and n-doping of PDTT3. IRAV range. Sequence: bottom to top.

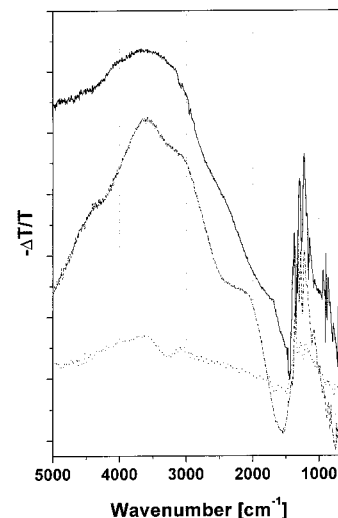


Figure 13. PIA-FTIR spectra of PDTT1 (dotted line), PDTT2 (dash-dotted line) and PDTT3 (solid line).

the corresponding p-doped polymer, especially concerning the IRAV bands. Such a similarity is implicit only for PDTT3, whose positive and negative charge carriers possess nearly identical IR signatures. For PDTT1 and PDTT2, which show different spectra in the p- and n-doped state, it must be inferred that mostly positive polarons are delocalized and behave as majority charge carriers in the photodoped material. Conversely, negative charges are probably trapped within certain sites of the polymer, e.g., chain defects, or localized in the repeating units themselves. These results are consistent with the higher p-type charge carrier delocalization in PDTT1 and PDTT2 found by the in-situ FTIR spectroelectrochemical measurements.

In all cases, no softening of IRAV modes is observed in the photoexcited spectra as compared to the electrochemical doping

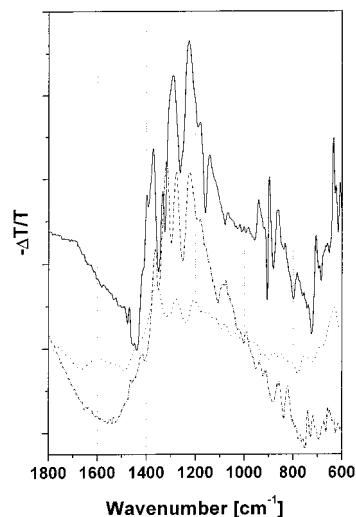


Figure 14. PIA-FTIR spectra of PDTT1 (dotted line), PDTT2 (dash-dotted line) and PDTT3 (solid line). Spectra are arbitrarily rescaled.

induced spectra. On the contrary, some bands even show a small blue-shift in the photoexcited case. This observation suggests that the small number of carriers generated by photodoping have a kind of “extra-pinning”, possibly arising from strongly localized negative charges acting as pinning sites for the positive carriers. Such an effect explains the similarity of the IRAV frequencies despite the absence of electrolyte counterions in the photoexcited case.

In our previous paper, we discussed the correlation between IRAV bands and Raman bands of PDTT3.³⁷ Here we extend the same analysis to PDTT1, as detailed in Table 1. The bands α_1 and α_2 , which in Raman show large intensity redistribution, and softening with excitation wavelength, exhibit further changes going to the IR spectra. α_1 weakens in the p-doped polymer spectrum and is observed only as shoulder in the PIA-FTIR spectrum. Conversely, α_2 , observed as a shoulder in the Raman spectrum with excitation at 457 nm, becomes stronger with the NIR excitation and is among the dominant bands in the doped and PIA-FTIR polymer spectra. In addition to the softening with increasing excitation wavelength, α_1 and α_2 show a further shift to red in the FTIR polymer spectra. For PDTT2, due to the complexity of the spectral pattern and especially to the overlapping of several bands in the p-doped polymer spectrum, such a correlation would be too speculative and has not been done. However, it can be noted that the sharp and medium band β_9 , observed in all of the IR as well as the Raman spectra of PDTT2, seems to have the same origin as γ_7 in PDTT3.³⁷

In situ Electron Spin Resonance Spectroscopy. In addition to vibrational spectroscopy, ESR spectra of PDTTs were recorded in situ during electrochemical p- and n-doping in potential scan experiments. In all cases, the formation of paramagnetic charge carriers (polarons) is observed. As an example, Figure 15 shows the ESR signal obtained during p-doping and dedoping of PDTT3. A detailed study of the behavior of the ESR signal and its correlation to electrochemical parameters (e.g., amount of charge, electrode potential) is in progress. The maximum signal obtained during p- and n-doping was used for the determination of the g -factors. The rescaled spectra of the respective charge carriers in PDTT1, PDTT2, and PDTT3 are shown in Figure 16. P-doped PDTTs spectra consist of a single line at g -factors around 2.004, which is higher than the values commonly observed for doped (as well as photoexcited) conjugated oligomers⁵² and polymers.^{53–56} The n-doped PDTTs spectra consist of a single line at even higher g -factors.

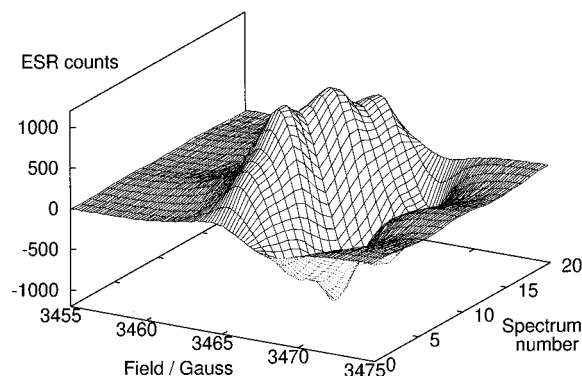


Figure 15. In situ ESR spectra during p-doping (spectrum number 0–10) and dedoping (11–20) of PDTT3.

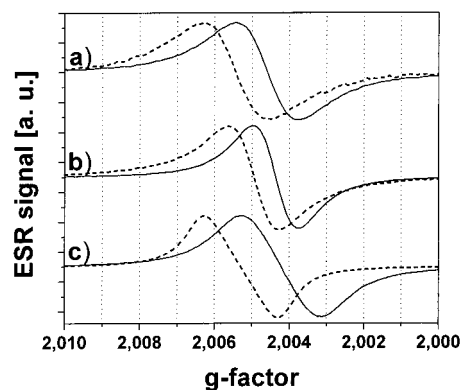


Figure 16. In situ ESR spectra of p- (solid line) and n-doped (dotted line) PDTT1 (a), PDTT2 (b), and PDTT3 (c). Spectra are arbitrarily rescaled.

TABLE 3: Position and Line Width of Doped PDTTs ESR Signals^a

	PDTT1	PDTT2	PDTT3
g -factor p/n	2.0045/2.0054	2.0044/2.0049	2.0042/2.0052
ΔH_{p-p} (G) p/n	2.7/2.8	2.0/2.2	3.6/3.3

The spin signature of negative polarons is seen by the lines at g -factor values ranging from 2.0049 (PDTT2) to 2.0054 (PDTT1). These g -factors are remarkably high. The origin of the high g -factors is assumed to be the stronger spin–orbit coupling within the PDTTs, potentially related to the sulfur atoms in the fused moieties, which again shows their strong influence of the polymer properties. It is also remarkable that the g -factor for the negative polaron as compared to the positive polaron on one-and-the-same polymer is systematically higher. This g -factor shift can have several origins:

–The different spin–orbit coupling terms by the different polaron distribution on the sulfur atoms in the p- and n-doped polymer.

–The differences in excited-state energies for the n- and p-polarons, respectively, resulting in different g -factor shift term due to the denominator in the spin–orbit terms.⁵⁷

–In principle, there could also be an effect due to the incorporation of different counterions during p- and n-doping.⁵⁸

Independently of the doping sign, all ESR lines are rather narrow (ΔH_{p-p} of 2–3.5 G). Narrow ESR lines for p-doped conducting polymers are commonly observed and interpreted by motional as well as exchange narrowing due to a large number of carriers.⁵⁹ Positions and widths of the ESR lines are listed in Table 3.

Conclusion

In this work, we have investigated the doped and pristine PDTTs, low band-gap polymers that undergo reversible electrochemical p- and n-doping as well as photodoping. In pristine PDTTs, the Raman modes mostly contributing to the ECC do undergo intensity redistribution as well as frequency dispersion. This behavior can be taken as a vibrational signature of the enhanced quinoidal character of the chain, which overcomes the π -electron confinement typical of simpler polythiophenes. In doped PDTT1 and PDTT2, charge carriers of opposite signs show different spectral signatures, whereas in doped PDTT3 no significant differences are observed. The spectral patterns are strongly affected by the different aromatic moieties fused to the thiophene rings forming the polythiophene-like chain. In particular, as their aromaticity increases and, thus, the polymer band-gap decreases, modes located within the fused moiety couple to the delocalized electron system along the polythiophene backbone.

With in situ ESR spectroelectrochemistry, paramagnetic charge carriers were observed upon both signs of doping. The spins of the positive carriers are found at g-factors higher than those reported for most of p-doped conjugated polymers. The spin of negative carriers exhibits a shift of the g-factors to even higher values as compared to the positive polarons.

Acknowledgment. C. J. Brabec and E. Ehrenfreund are gratefully acknowledged for the valuable discussions. We thank M. C. Scharber for help with the ESR studies. The financial support of the Austrian Foundation for the Advancement of Science (FWF P-12680 CHE) as well as the financial support of the European Commission (RTN, Euromap project) is acknowledged.

References and Notes

- (1) *Handbook of Conducting Polymers*, 2nd ed.; Skotheim, T. A.; Elsenbaumer R. L.; Reynolds, J. R.; Eds.; Marcel Dekker: New York, 1998.
- (2) Yokonuma, N.; Furukawa, Y.; Tasumi, M.; Kuroda, M.; Nakayama, J. *Chem. Phys. Lett.* **1996**, *255*, 431.
- (3) *Semiconducting Polymers, Chemistry Physics and Engineering*; Hadziioannu G., van Hutten P. F., Eds.; Wiley: Weinheim, 2000.
- (4) *Primary Photoexcitations in Conjugated Polymers: Molecular Exciton versus Semiconductor Band Model*, Sariciftci, N. S., Ed.; World Scientific: Singapore, 1997.
- (5) Sariciftci, N. S.; Smilowitz, L.; Heeger, A. J.; Wudl, F. *Science*, **1995**, *270*, 1474.
- (6) See for instance Del Zoppo, M.; Castiglioni, C.; Zuliani, P.; Zerbi, G. In *Handbook of Conducting Polymers*, 2nd ed.; Skotheim, T. A., Elsenbaumer, R. L., Reynolds, J. R., Eds.; Marcel Dekker: New York, 1988; Chapter 28, and references therein.
- (7) See, for instance: Zagorska, M.; Pron, A.; Lefrant, S. In *Handbook of Conductive Molecules and Polymers*, 2nd ed.; Nalwa, H. S., Ed.; Wiley: Chichester, 1997; Vol. 3, Chapter 4, and references therein.
- (8) Horowitz, B. *Solid State Commun.* **1982**, *41*, 729.
- (9) Ehrenfreund, E.; Vardeny, Z. V.; Brafman, O.; Horowitz, B. *Phys. Rev. B* **1987**, *36*, 1535.
- (10) Castiglioni, C.; Gussoni, M.; Lopez Navarrete, J. T.; Zerbi, G. *Solid State Comm.* **1988**, *36*, 1535.
- (11) Zerbi, G.; Gussoni, M.; Castiglioni, C. In *Conjugated Polymers*; Brédas, J. L.; Silbey, R., Eds.; Kluwer: Dordrecht, 1991; p 435.
- (12) Girlando, A.; Painelli, A.; Soos, Z. G. *J. Chem. Phys.* **1993**, *98*, 7459.
- (13) Ehrenfreund, E.; Vardeny, Z. V. *Proc. SPIE* **1997**, *3145*, 324.
- (14) Agosti, E.; Rivola, M.; Hernandez, V.; Del Zoppo, M.; Zerbi, G. *Synth. Met.* **1999**, *100*, 101.
- (15) Gussoni, M.; Castiglioni, C.; Zerbi, G. In *Spectroscopy of Advanced Materials*; Clark, R. J. H., Hester, R. E., Eds.; Wiley: New York, 1991; p 251.
- (16) Arbizzani, C.; Catellani, M.; Mastragostino, M.; Cerroni, M. G. *J. Electroanal. Chem.* **1997**, *423*, 23.
- (17) Arbizzani, C.; Catellani, M.; Cerroni, M. G.; Mastragostino, M. *Synth. Met.* **1997**, *84*, 249.
- (18) Bolognesi, A.; Catellani, M.; Destri, S.; Porzio, W. *Mol. Cryst. Liq. Cryst.* **1990**, *187*, 259.
- (19) Taliani, C.; Ruani, G.; Zamboni, R.; Bolognesi, A.; Catellani, M.; Destri, S.; Porzio, W.; Ostojica, P. *Synth. Met.* **1989**, *28*, C507.
- (20) Bolognesi, A.; Catellani, M.; Destri, S.; Ferro, D. R.; Porzio, W. *Synth. Met.* **1989**, *28*, C527.
- (21) Catellani, M.; Lazzaroni, R.; Luzzati, S.; Brédas, J. L. *Synth. Met.* **1999**, *101*, 175.
- (22) Cava, M. P.; Latshmikantam, M. V. In *Comprehensive Heterocyclic Chemistry, the Structure, Reactions, Synthesis and Uses of Heterocyclic Compounds*, 1st ed.; Bird, C. W., Cheeseman, G. W. H., Eds.; Pergamon Press: Oxford, 1984; Vol. 4, p 1040.
- (23) Gutman, I.; Milun, M.; Trinajstić, N. *J. Am. Chem. Soc.* **1977**, *99*, 692.
- (24) Brédas, J. L. *Mol. Cryst. Liq. Cryst.* **1985**, *49*, 118.
- (25) Patil, O.; Heeger, A. J.; Wudl, F. *Chem. Rev.* **1988**, *88*, 183.
- (26) Kertesz, M. In *Handbook of Conductive Molecules and Polymers*; Nalwa, H. S., Ed.; Wiley: Chichester, 1997; Vol. 4, Chapter 3.
- (27) Neudeck, A.; Petr, A.; Dunsch, L. *Synth. Met.* **1999**, *107*, 143.
- (28) Neudeck, A.; Petr, A.; Dunsch, L. *J. Phys. Chem. B.* **1999**, *103*, 912.
- (29) Rapta, P.; Petr, A.; Dunsch, L.; Ivaska, A. *Synth. Met.* **2001**, *119*, 409.
- (30) Petr, A.; Kvarnström, C.; Dunsch, L.; Ivaska, A. *Synth. Met.* **2000**, *108*, 245.
- (31) De Jong, F.; Janssen, M. J. *J. Org. Chem.* **1971**, *36*, 1945.
- (32) De Jong, F.; Janssen, M. J. *J. Org. Chem.* **1971**, *36*, 1998.
- (33) Neugebauer, H.; Sariciftci, N. S. In *Lower Dimensional Systems and Molecular Electronics*, Nato ASI series, Series B: Physics, Vol. 248; Metzger, R. M.; Day, P.; Papavassiliou, G. C., Eds.; Plenum Press: New York, 1991; p 401.
- (34) Neugebauer, H. *Macromol. Symp.* **1995**, *94*, 61.
- (35) Kvarnström, C.; Neugebauer, H.; Ivaska, A. In *Advanced Functional Molecules and Polymers*, 4 Volumes; Nalwa, H. S., Ed.; Gordon & Breach: Langhorne, PA, 2001; Vol. 2, Ch. 3.
- (36) Dunsch, L.; Petr, A. *Ber. Bunsen-Ges. Phys. Chem.* **1993**, *97*, 436.
- (37) Cravino, A.; Neugebauer, H.; Luzzati, S.; Catellani, M.; Sariciftci, N. S. *J. Phys. Chem. B* **2001**, *105*, 46.
- (38) Pron, A.; Louarn, G.; Lapkowsky, M.; Zagorska, M.; Glowczyk-Zubek, J.; Lefrant, S. *Macromolecules* **1995**, *28*, 4644.
- (39) Louarn, G.; Trznadel, M.; Buisson, J. P.; Laska, J.; Pron, A.; Lapkowsky, M.; Lefrant, S. *J. Phys. Chem.* **1996**, *100*, 1232.
- (40) See ref 6, p 768 and pp 799–800 (Raman lines B, C, D).
- (41) Simonet, J.; Rault-Berthelot, J. *Prog. Solid State Chem.* **1991**, *21*, 1.
- (42) Zotti, G. In *Handbook of Conductive Molecules and Polymers*, 2nd ed.; Nalwa, H. S., Ed.; Wiley: Chichester, 1997; Vol. 2, Chapter 4.
- (43) Kvarnström, C.; Neugebauer, H.; Blomquist, S.; Ahonen, H. J.; Kankare, J.; Ivaska, A.; Sariciftci, N. S. *J. Mol. Struct.* **2000**, *521*, 271.
- (44) Kvarnström, C.; Neugebauer, H.; Blomquist, S.; Ahonen, H. J.; Kankare, J.; Ivaska, A.; Sariciftci, N. S. *Synth. Met.* **1999**, *101*, 66.
- (45) Neugebauer, H.; Kvarnström, C.; Cravino, A.; Yohannes, T.; Sariciftci, N. S. *Synth. Met.* **2001**, *116*, 115.
- (46) Neugebauer, H.; Kvarnström, C.; Brabec, C. J.; Sariciftci, N. S.; Kiebooms, R.; Wudl, F.; Luzzati, S. *J. Chem. Phys.* **1999**, *111*, 1039.
- (47) Balberg, I.; Naidis, R.; Lee, M.-K.; Shinar, J.; Fonseca, L. F. *Appl. Phys. Lett.* **2001**, *79*, 197.
- (48) Yu, G.; Gao, J.; Hummelen, J. C.; Wudl, F.; Heeger, A. J. *Science* **1995**, *270*, 1789.
- (49) Wang, Y. *Nature* **1992**, *356*, 585.
- (50) Neugebauer, H.; Neckel, A.; Brinda-Konopik, N. In *Electronic Properties of Polymers and Related Compounds*; Kuzmany, H., Mehring, M., Roth, S., Eds.; Solid State Sci. 63, Springer: Heidelberg, 1985; p 227.
- (51) Moses, D.; Dogariu, A.; Heeger, A. J. *Synth. Met.* **2001**, *111*, 19.
- (52) Simmoneau, A.; Chauvet, O.; Molinié, P.; Froyer, G. *Synth. Met.* **1997**, *84*, 657.
- (53) Sebt, M.; Merlin, A.; Ghanbaja, J.; Billaud, D. *Synth. Met.* **1997**, *84*, 665.
- (54) Dyakonov, V.; Zorinyants, G.; Scharber, M. C.; Brabec, C. J.; Janssen, R. A. J.; Hummelen, J. C.; Sariciftci, N. S. *Phys. Rev. B* **1999**, *59*, 8019.
- (55) Chandrasekhar, P. *Conducting Polymers, Fundamentals and Applications. A Practical Approach*; Kluwer Academic: Norwell, 1999; pp 315–322.
- (56) *Handbook of Conductive Molecules and Polymers*, 2nd ed.; Nalwa, H. S., Ed.; Wiley: Chichester, 1997; Vol. 3, Ch. 3.
- (57) Weil, J. A.; Bolton, J. R.; Wertz, J. E. *Electron Paramagnetic Resonance, Elementary Theory and Practical Applications*; Wiley: New York, 1994.
- (58) Salem, L. *The Molecular Orbital Theory of Conjugated Systems*; W. A. Benjamin: Reading, 1966; Ch. 5.
- (59) Mizoguchi, K.; Kuroda, S. In ref 56, p 251.